# High-speed signal propagation on lossy transmission lines

by A. Deutsch

G. V. Kopcsay

V. A. Ranieri

J. K. Cataldo

E. A. Galligan

W. S. Graham

R. P. McGouey

S. L. Nunes

J. R. Paraszczak

J. J. Ritsko

R. J. Serino

D. Y. Shih

J. S. Wilczynski

This paper addresses some of the problems encountered in propagating high-speed signals on lossy transmission lines encountered in highperformance computers. A technique is described for including frequency-dependent losses, such as skin effect and dielectric dispersion, in transmission line analyses. The disjoint group of available tools is brought together, and their relevance to the propagation of high-speed pulses in digital circuit applications is explained. Guidelines are given for different interconnection technologies to indicate where the onset of severe dispersion takes place. Experimental structures have been built and tested, and this paper reports on their electrical performance and demonstrates the agreement between measured data and waveforms derived from analysis. The paper

<sup>©</sup>Copyright 1990 by International Business Machines Corporation. Copying in printed form for private use is permitted without payment of royalty provided that (1) each reproduction is done without alteration and (2) the *Journal* reference and IBM copyright notice are included on the first page. The title and abstract, but no other portions, of this paper may be copied or distributed royalty free without further permission by computer-based and other information-service systems. Permission to *republish* any other portion of this paper must be obtained from the Editor.

addresses the problems found on lossy lines, such as reflections, rise-time slowdown, increased delay, attenuation, and crosstalk, and suggests methods for controlling these effects in order to maintain distortion-free propagation of high-speed signals.

#### Introduction

The advances being made in circuit density and speed, both at the chip and package level, are placing increasing demands on the performance of interconnection technologies. Designers are reducing the wiring cross sections and trying to pack the lines closer together, while at the same time the propagated signals switch with faster rise times. New insulators with lower dielectric constants and improved thermal properties and conductors with lower resistivity are extending operation to higher speeds. All these challenges are bringing into focus the need to understand pulse distortions caused by loss mechanisms such as skin effect and dielectric dispersion. Interconnection performance is more and more limited by the ability to control reflections caused by discontinuities in the signal paths, such as vias, crossing lines, wire bonds, and connectors; it is also limited by the higher level of crosstalk and switching-induced noise due

to the packing density and speed increase.

Table 1 Review of packaging technologies.

Interconnection type	Line width (µm)	Wiring resistance (Ω/cm)	Maximum interconnection length (cm)
On-chip	1-2	130-260	0.7-1.4
Thin-film carriers	10-25	1.25-4	20-45
Ceramic	75-100	0.4-0.7	20-50
Printed-circuit boards	60-100	0.06-0.08	40-70

Reducing wiring dimensions results in appreciably resistive lines, even when the best conductive metals, such as copper, are used. High-speed signal propagation and the use of lossy transmission lines are narrowing the gap between digital and microwave circuit designers. Transient analysis of coupled lossy lines having frequency-dependent parameters becomes a necessity. Although some of the analysis techniques we use have been available for many years, they have not been applied extensively to modeling high-speed pulses in digital circuit environments. The circuit-to-circuit interconnection in today's high-performance computers has many varieties, as shown in Table 1 [1, 2]. Signals on these carriers have rise times of  $t_r = 100$  to 1000 ps. It is important to be able to determine the maximum usable length  $(l_{max})$  for high-speed pulse propagation in these configurations and know its dependence on the signal line resistance per unit length (R).

In this paper, we address some of the problems encountered in propagating high-speed signals on lossy transmission lines. We suggest guidelines for applying different analysis techniques of the various loss mechanisms, for a range of computer packaging interconnection technologies encountered today, such as those illustrated in Table 1. We describe modeling techniques used for accurate characterization of electrical performance and discuss their application to several transmission line structures. We describe measurements of high-speed signal propagation on lossy lines, which were made on experimental structures using a highbandwidth test system. We compare experimental and simulated effects of delay, crosstalk, and rise-time degradation due to dispersion introduced by skin effect, attenuation, and dielectric loss.

# Theoretical background

For a uniform transmission line, the differential equations for the line voltage V and current I can be expressed in the frequency domain as follows [3]:

$$\frac{dV}{dx} = -ZI,\tag{1}$$

$$\frac{dI}{dx} = -YV,\tag{2}$$

where  $Z = R + j\omega L$  and  $Y = G + j\omega C$ . R, L, C, and G are the line resistance, inductance, capacitance, and dielectric conductance per unit length and are in general frequency-dependent. A quasi-TEM behavior can be assumed for typical interconnection geometries, since the transmission line cross section is a small fraction of the wavelength in the frequency range of interest. The general solution to Equations (1) and (2) can be expressed as

$$V = V_{A}e^{-\Gamma_{X}} + V_{B}e^{\Gamma_{X}}, \tag{3}$$

$$I = I_{\mathsf{A}} e^{-\Gamma_{\mathsf{X}}} + I_{\mathsf{B}} e^{\Gamma_{\mathsf{X}}},\tag{4}$$

where the propagation constant is defined as

$$\Gamma = \sqrt{ZY} = \sqrt{(R + j\omega L)(G + j\omega C)},$$
 (5)

and the characteristic impedance is

$$Z_0 = \sqrt{\frac{Z}{Y}} = \sqrt{\frac{R + j\omega L}{G + j\omega C}},$$
 (6)

as shown in [3].  $V_A$ ,  $V_B$ ,  $I_A$ , and  $I_B$  are constants that can be determined by boundary conditions at the two ends of the line. The propagation constant  $\Gamma$  can also be written as  $\alpha + j\beta$ , where  $\alpha = \text{Re }\Gamma$  is the attenuation constant and  $\beta = \text{Im }\Gamma$  is the phase constant.

In the case of no losses, R=G=0, the voltage at all points along a line has the same amplitude, and it is shifted in time with a propagation delay per unit length  $\tau$  of  $\beta/\omega=\sqrt{LC}$ . The characteristic impedance for the lossless case is  $Z_0=\sqrt{L/C}$ .

In the case when losses are small but not negligible (R and G are sufficiently small that  $R/L \ll \omega$  and  $G/C \ll \omega$ ), the attenuation and phase constant per unit length, according to [3], can be approximated by

$$\alpha = \frac{R}{2\sqrt{L/C}} + \frac{G}{2}\sqrt{\frac{L}{C}},\tag{7}$$

$$\beta = \omega \sqrt{LC} + \left(\frac{R}{2\sqrt{L/C}}\right) \frac{R}{4\omega L}$$

$$+\left(\frac{G}{2}\sqrt{\frac{L}{C}}\right)\frac{G}{4\omega C} - \frac{RG}{4\omega\sqrt{LC}}.$$
 (8)

If the series resistive loss is small but finite, some pulse distortion will be encountered, because the different frequency components will attenuate the same amount but will be shifted in phase differently, and the rise time will be degraded by dispersion. For interconnections with maximum length  $l_{\rm max}$ , if  $Rl_{\rm max} \ll Z_0$ , dispersion is usually negligible, and the total signal line resistance results in a dc drop, since the lines are generally terminated in their

characteristic impedance. For example, a printed circuit line with  $R=0.06~\Omega/\mathrm{cm}$  and  $l_{\mathrm{max}}$  as large as 70 cm,  $Rl_{\mathrm{max}}=4.2~\Omega$ , which is one twentieth of  $Z_0$  ( $Z_0=80~\Omega$  generally), will transmit signals without significant distortion. This is valid when G, and therefore dielectric loss, is negligible.

In the general case, where both attenuation and phase velocity depend on frequency, the resulting rise-time dispersion is more pronounced. Guidelines are given below for different technologies, to indicate the speeds and density levels where such losses become important. The attenuation, expressed in decibels per unit length, can be derived in a general form as follows:

$$ATTEN = 20 \log_{10} e^{\text{Re}\Gamma}, \tag{9}$$

where  $\Gamma$  has the form given in (5). If the medium in which the conductors are located has finite losses, then the dielectric constant  $\varepsilon$  must be replaced by  $\varepsilon(1-j\tan\delta_1)$  [4] in calculations of C and G, where  $\tan\delta_1$  is the loss tangent of the material. The effective conductivity of the material is  $\sigma$ , where  $\sigma = \omega \varepsilon \tan\delta_1$ . The shunt conductance G is then given by  $G = \sigma C/\varepsilon = \omega C \tan\delta_1$ . Then  $\Gamma$  can be expressed as

$$\Gamma = \sqrt{(R + j\omega L)(G + j\omega C)}$$

$$= \sqrt{-\omega^2 L C(1 - jR/\omega L)(1 - j\tan \delta_i)}, \qquad (10)$$

and Equation (9) for attenuation, in decibels per unit length, becomes

ATTEN

$$= 20 \log_{10} \exp \left( \omega \sqrt{LC \sqrt{\left[1 + (R/\omega L)^{2}\right]\left[1 + (\tan \delta_{l})^{2}\right]}} \right)$$

$$\times \sin \left( \frac{\tan^{-1} \left\{ (R/\omega L + \tan \delta_{l}) / \left[1 - (R/\omega L) \tan \delta_{l}\right] \right\}}{2} \right)$$

and can be used to calculate frequency-dependent resistive and dielectric losses on a single line.

#### Skin-effect losses

At high frequencies the loss due to skin effect becomes important. Current crowding on the surface of the conductor increases its effective resistance, and the conductor exhibits an internal inductance,  $L_{\rm int}$ , due to magnetic flux penetration, in addition to the external inductance. The penetration of the wave into the conductor as it propagates along the surface causes a reduction in phase velocity and an increase in series impedance and attenuation. The skin depth  $\delta$  is defined as the penetration distance at which the current density is attenuated by 1 neper (1/e = -8.7 decibels) and is equal [5] to

$$\delta = \sqrt{\frac{\rho}{\pi f \mu}},\tag{12}$$

where f,  $\rho$ , and  $\mu$  are the frequency, conductor resistivity, and permeability of the medium, respectively. For an arbitrary solid conductor, the skin effect results in a surface resistance,  $R_{\rm S}$ , and reactance,  $X=\omega L_{\rm int}$ , which are both frequency-dependent and, in general, not equal. At sufficiently high frequency, the skin depth is much smaller than the conductor cross-sectional dimensions. Then,  $R_{\rm S}\cong X$  [5], and the additional series impedance due to skin effect is proportional to the square root of the frequency.

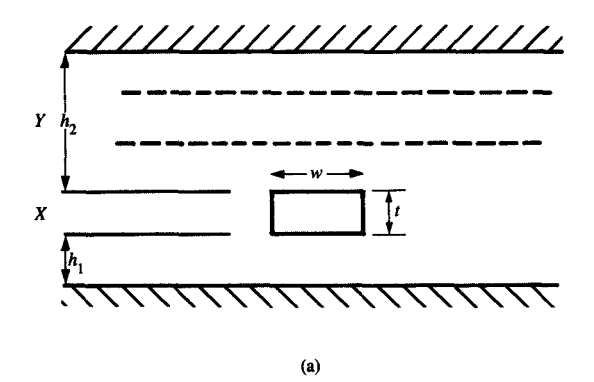
At low frequencies, the skin depth is much larger than the conductor cross section t (for typical strip lines, t is usually taken to be the smaller dimension). The current approaches uniform distribution, and the resistance  $R \cong R_{dc}$ . As the frequency increases,  $\delta$  becomes smaller than the cross section t, and both R and L are frequencydependent. In this mid-frequency range, R(f) and L(f)can be calculated by using the numerical technique described in [6], which is efficient for rectangular conductors. According to this method, strip line conductors and grounds are divided into parallel segments having dimensions smaller than the skin depth, such that the current density can be assumed constant throughout each segment. To accurately model strip line conductors, one should use enough segments to account for current crowding near the edges of the conductor as well as the current penetration. The finite-element method [7] could also be used to determine R(f) and L(f) in this frequency range. An example is given in [8].

# • Comparison of analysis techniques

At high frequencies, the technique described in [6] and the finite-element method [7] both require excessive computer time, because of the large number of elements needed to achieve accuracy when the skin depth is much less than the conductor cross section. When  $\delta \ll t$  (as a guideline,  $\delta \leq 0.1$  t), a very simple method developed by H. Wheeler [5] in 1942 (the "incremental inductance rule") is applicable. This rule states that the effective resistance in a circuit is equal to the change of reactance caused by the penetration of magnetic flux into the conductor. The resistance R is that of a layer whose thickness is  $\delta$ , while the internal inductance is due to the flux penetration of  $\sigma/2$ . This is equivalent to assuming that the surface of the conductor recedes by  $\delta/2$ . Thus R(f) and L(f) can be calculated as follows [5]:

$$R(f) = R_{\rm S}(f) = \omega \frac{\delta}{2} \frac{\partial L}{\partial n},$$
 (13)

$$L(f) = L_{\text{ext}} + L_{\text{int}}(f) = L_{\text{ext}} + \frac{\delta}{2} \frac{\partial L}{\partial n}, \tag{14}$$



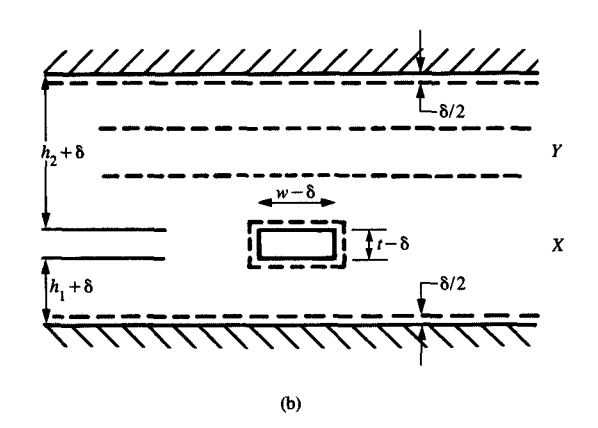


#### Figure 1

Cross sections used for calculating the change of inductance  $(\partial L/\partial n)$  term for X- and Y-directed signal lines: (a) Triplate structure with X-layer conductor of width w and thickness t. (b) Same structure with X-layer conductor of width  $w-\delta$  and thickness  $t-\delta$ .

where n is the direction normal to the surface and  $L_{\rm ext}$  is the external circuit inductance (i.e.,  $L_{\rm ext}$  is frequency-independent and associated with the magnetic field surrounding the conductors).

In the case where X- and Y-directed signal lines are placed between two reference planes, the change of inductance  $\partial L/\partial n$  can be calculated using the two cases shown in **Figure 1**. Capacitance of X-layer conductors is obtained using the method described in [9], which considers only the surface charge density (zero depth of penetration). External inductance is then obtained from the relation  $LC = \varepsilon \mu$ , calculated in free space. The capacitance calculation is made first for the conductor of width w, thickness t, and separations  $h_1$  and  $h_2$  from the top and bottom reference planes [Figure 1(a)]. All the surfaces are then considered to be recessed by  $\delta/2$ , and

the calculation is repeated for the cross section in Figure 1(b) with the conductor of width  $w-\delta$  and thickness  $t-\delta$  separated by  $h_1+\delta$  and  $h_2+\delta$  from the ground planes. The difference in inductance is  $\partial L/\partial n$  for  $\partial n = \delta/2$ . It should be noted that this technique accurately takes into account edge effects and proximity to adjacent conductors and ground planes. Once the  $\partial L/\partial n$  term is obtained, R and L can be calculated for the high-frequency range of interest, using Equations (12), (13), and (14). Often a more approximate formula is used for resistance [10]:

$$R = \frac{\rho}{2(w+t)\delta},\tag{15}$$

which, compared to (13), underestimates R because it ignores the actual current distribution change due to the above effects.

We have found that reasonable results can be obtained by using the following approximations:

$$R(f) = \begin{cases} R_0 \sqrt{f} & \text{for high frequencies,} \\ R_{dc} & \text{for low frequencies;} \end{cases}$$
 (16)

$$L(f) = \begin{cases} L_{\text{ext}} + \frac{L_0}{\sqrt{f}} & \text{for high frequencies,} \\ L_{\text{dc}} & \text{for low frequencies.} \end{cases}$$
 (17)

In particular, these approximations are useful for modeling transient pulse propagation, where the excitation consists of a broad-band frequency spectrum; they are relatively insensitive to small inaccuracies in R and L near the intersections of the high- and low-frequency curves. This approximation is, of course, not accurate in the transition frequency region ( $\delta \approx t$ ). However, for a wide range of practical cases, time-domain pulse waveforms calculated with this simple method have been found to agree quite well with those obtained by using accurate, frequency-dependent R and L that are determined numerically.

At frequency low enough that  $R\gg \omega L$ , accurate determination of  $L_{\rm dc}$  is not necessary. This is particularly important when considering lines with infinite ground planes, for which the low-frequency inductance decreases logarithmically, while the series impedance is mostly resistive and well defined. The constants  $R_0$  and  $L_0$  are calculated using the incremental inductance rule. One should be cautious about using this approximation when a large portion of the excitation pulse spectrum is expected to fall in the transition frequency region.

For highly resistive interconnections, skin effect will dominate; therefore, the dielectric loss can be ignored for most practical digital circuit-switching speeds. In the case of wiring with small R, the dielectric loss should be included in the analysis. Note that for constant  $\tan \delta_1$ ,

dielectric loss increases in proportion to frequency and will therefore always be significant for fast enough pulse rise times. Experimental results shown in the following sections illustrate the significance of the various loss mechanisms.

# **Resistive losses**

#### • Frequency-independent losses

It is shown in [11] that the solution to Equations (1) and (2) for an infinitely long, lossy line excited by a unit step function can be expressed in the time domain as follows:

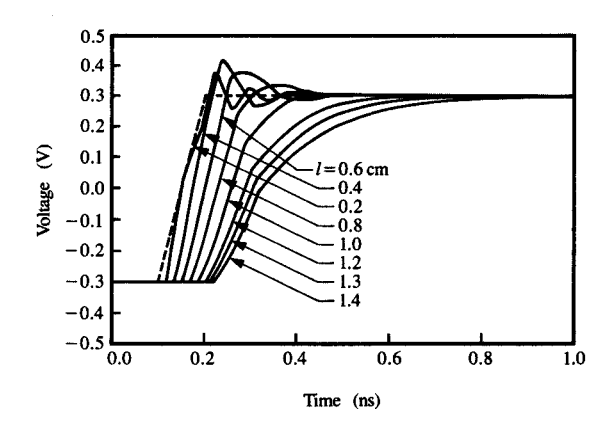
$$V(l, t)$$

$$= \left\{ e^{-Rl/2Z_0} + \frac{Rl}{2Z_0} \int_{\tau=l\sqrt{LC}}^{t} \frac{e^{-Rl/2Z_0}}{\sqrt{\tau^2 - (l\sqrt{LC})^2}} \right.$$

$$\times I_1 \left[ \frac{R}{2Z_0} \sqrt{(\tau/\sqrt{LC})^2 - l^2} \right] d\tau \right\} u(t - l\sqrt{LC}) \qquad (18)$$
for  $t \ge l\sqrt{LC}$ ,

where u(t) is a unit step function and  $I_1$  is a slowly rising modified Bessel function. The lossy line then behaves like a fast-rising LC line (the first term) and a slow RC line combined. Reference [12] recommends using such transmission lines without terminating resistors in order to take advantage of the voltage doubling that occurs due to reflection at the end of an open line. When RL is sufficiently small that the first term in (18) dominates, the attenuated pulse amplitude is restored at the far end of the line without significant rise-time degradation [13, 14]. If Rl becomes too large, the second term dominates, and the rise time deteriorates to that of a slow RC circuit. A design guideline is given in [12] for using such lines with  $l_{\max} \leq 2Z_0/R$  so that the attenuation  $e^{-Rl/2Z_0}$  will be less than or equal to 36.8%.

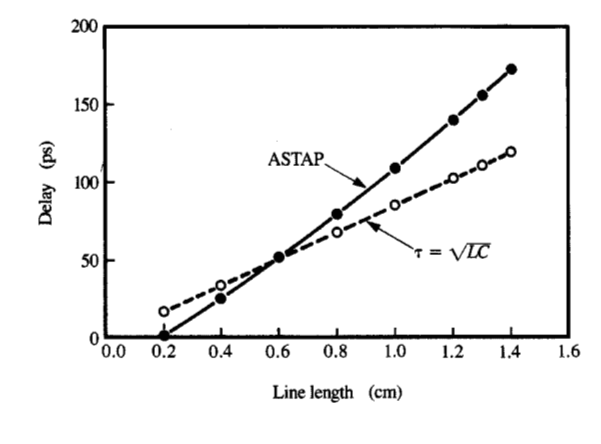
A typical example in which lossy line effects become important is on-chip wiring for fast-switching circuits with long interconnections (large chips). Aluminum lines have very high resistive losses, but the skin depth is much larger than the conductor cross sections for the typical frequency range of interest. For interconnections with  $\rho$ from 2 to 4  $\mu\Omega$ -cm, widths w from 1 to 2  $\mu$ m, and t from 1 to 1.4  $\mu$ m, the frequency at which skin-effect losses become important ( $\delta \le t$ ) starts at 50 to 100 GHz, or less than 10-ps rise times. Even for 100-ps rise-time signals, which contain frequency components with significant energy around 3 GHz, for which the skin depth  $\delta$  is 1.6 μm and is larger than the line thickness, the current density can be considered to be uniform. Rise-time dispersion for this case is dominated by frequencyindependent, series resistive losses. Propagation delay per unit length is greatly increased by other effects, such as

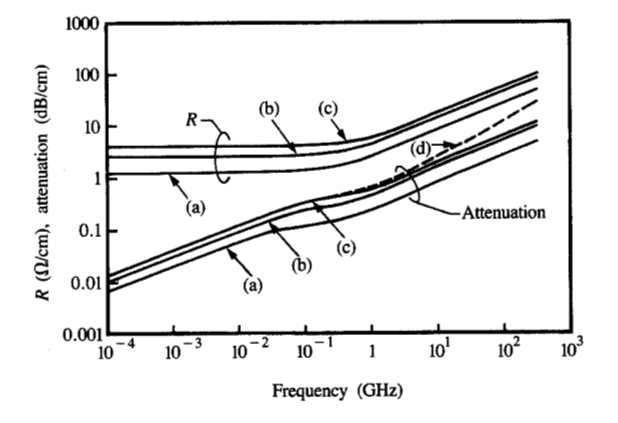


#### e Statille 2

On-chip signal propagation modeled for 100-ps rise-time source signal (dashed curve), with unterminated wiring lengths l=0.2 to 1.4 cm.

capacitive loading of adjacent orthogonal lines and increased inductance due to nonuniform power bus layouts. A typical calculated propagation delay  $(\tau = \sqrt{LC})$  is about 85 ps/cm, which is higher than the ideal value ( $\tau = \sqrt{\varepsilon_r}/c$ ) of 65.8 ps/cm for a dielectric with  $\varepsilon_r = 3.9$ , where  $\varepsilon_r$  is the relative dielectric and c is the velocity of light. According to the guideline given above, the maximum useful length  $l_{\text{max}}$  of this circuit-to-circuit wiring, which is usually unterminated, is about  $2Z_0/R = 2 \times 50 \Omega/130 \Omega/\text{cm} = 0.769 \text{ cm}$ . In the case of the longer lines that can be encountered on 1 to 1.4-cm chips, the propagation delay increases exponentially (rather than linearly) due to the RC line behavior. Signal propagation for a 100-ps rise-time source (dashed curve) for various lengths (l = 0.2 to 1.4 cm) of unterminated lines is illustrated in Figure 2. It was modeled using the ASTAP (Advanced Statistical Analysis Program) transient circuit analysis program [15], which takes into account the resistive line losses. In the case of very short lines that have propagation delay much less than the rise time, the delay measured at the 50% threshold is found to be less than the ideal  $\tau l = \sqrt{\varepsilon_r/c}$ ; this effect is due to the doubling of the signal at the unterminated end. In this case, most of the waveforms have only small overshoots, due to the negative reflection at the lowimpedance source and the fact that the slowly rising signal  $(t > \tau l)$  never reaches full amplitude at the line end before it doubles. The long lines  $(l > t_r/\tau)$ , however, start showing the RC behavior, since  $l > l_{max}$ . Figure 3 shows the exponentially increasing propagation delay for the modeled waveforms (solid curve) compared with the





#### 37.77

Propagation delay for on-chip interconnections modeled with ASTAP (solid curve) and calculated (dashed curve) for  $\tau = \sqrt{LC} = 85$  ps/cm.

**Table 2** Characteristics of analyzed transmission lines.

Туре	Thickness, t (µm)	Resistivity, ρ (μΩ-cm)	Resistance, $R_{dc}$ ( $\Omega$ /cm)
1	8	2	1.25
2	9	1.83	2.62
3	5.85	1.89	4

ideal calculated delay (dashed curve) with constant  $\tau = \sqrt{LC}$ . The exponential effect can be deduced from (18) for large Rl. As circuit speeds increase such that  $\delta < t$ , skin-effect losses should be included in this type of interconnection.

In the case of chip-to-chip wiring, the interconnection delays are much longer than the signal rise times, even though these transitions are slower than on-chip. In the case of a 100-mm multi-chip carrier [16],  $l_{\rm max}$  can approach 20 cm, and if the resistance R is in the range 1.25 to 4  $\Omega$ /cm, unterminated connections should be used, as is recommended in [12]. It is shown in [13] that since the resistive loss is very small for short lines (but long enough to have propagation delay greater than the rise time), the line behaves like an LC line [first term in (18)], and sustained reflections from both ends generate unwanted over- and under-shoots. An active clamp network, such as one using Schottky barrier diodes, can be used to suppress the oscillations and maintain a fixed steady-state level at one tenth the current needed for a terminating resistor. This clamp should be designed to have an equivalent impedance matched to the line  $Z_0$  at the moment of turn-on.

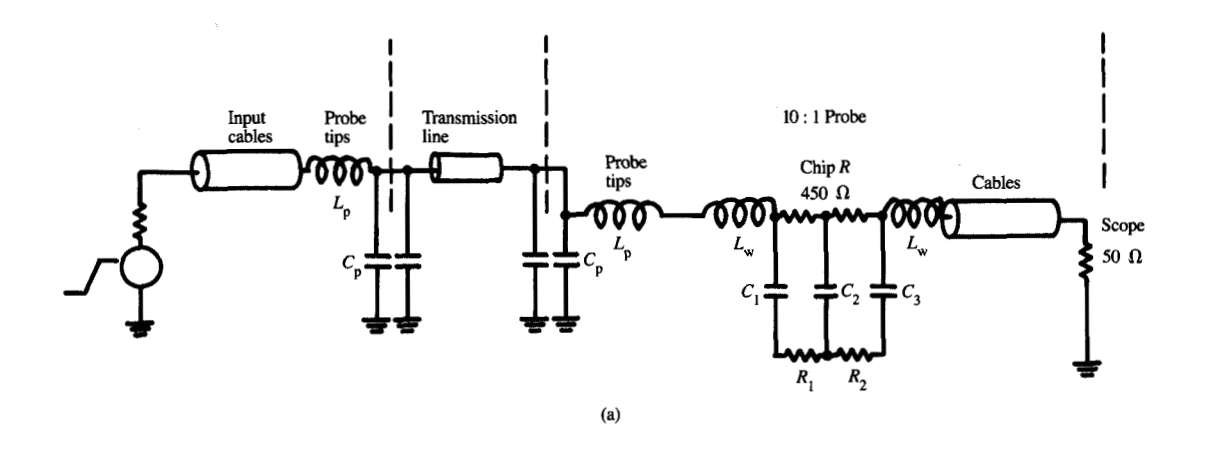
#### Figure 2

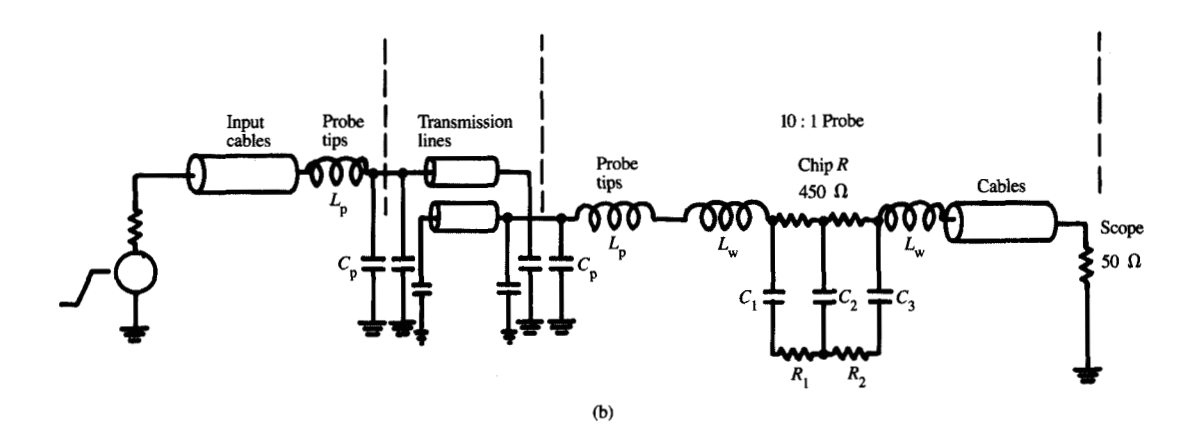
Calculated frequency dependence of resistance and attenuation for lines with  $R_{\rm dc}=$  (a) 1.25, (b) 2.62, (c) 4  $\Omega$ /cm. (d) Attenuation for line with  $R_{\rm dc}=$  4  $\Omega$ /cm and tan  $\delta_1=0.03$ .

#### • Frequency-dependent losses

To illustrate the frequency-dependent properties encountered in typical chip-to-chip interconnections, resistance R(f) and inductance L(f) were calculated for lines having a range of resistive loss. The characteristics of three line types that were measured and analyzed are summarized in Table 2. The cross section of these transmission lines was the triplate structure shown in Figure 1, consisting of X and Y signal lines between two ground planes. The method outlined above, using a combination of the numerical technique [6] and Wheeler's rule [5], was employed. The frequencydependent line parameters R(f) and L(f) were substituted in Equation (11) to obtain the attenuation curves shown in Figure 4 with solid lines. Dielectric loss has been neglected (tan  $\delta_1 = 0$ ). The transition frequencies where skin effect becomes significant ( $\delta \leq 0.3t$ ) were  $f_1 = 0.7 \text{ GHz}, f_2 = 0.5 \text{ GHz}, \text{ and } f_3 = 1.25 \text{ GHz}, \text{ with the}$ attenuation levels of  $ATTEN_1 = 0.2$  dB/cm,  $ATTEN_2 =$ 0.36 dB/cm, and  $ATTEN_3 = 0.46 \text{ dB/cm}$ .

Although dielectric loss increases in proportion to frequency, since  $G = \omega C \tan \delta_1$ , most good insulators have very small  $\tan \delta_1$ , so that the series resistive losses dominate. If the dielectric loss is included in our calculation of the frequency-dependent attenuation and a large value of loss is assumed, such as  $\tan \delta_1 = 0.03$ , curve (d) is obtained in Figure 4 for the type 3 line with  $R_{\rm dc} = 4 \Omega/{\rm cm}$ . At 14 GHz (where  $\delta = 0.1t$  and skin effect is significant), the calculated attenuation increases from 2.4 to 3.25 dB/cm. Substantial increase is seen only at f = 316 GHz, from 11.9 to 30.2 dB/cm. Such high frequencies are very seldom of interest in digital





#### Flattre 5

Equivalent circuit representation of 19-GHz-bandwidth high-impedance test system for measuring (a) propagation on single line and (b) far-end crosstalk for two coupled lines.

computer circuits, where the energy of these high-frequency components in the spectrum of practical rise times of 200–1000 ps is very small. The tan  $\delta_1 = 0.03$  value used, although high, could be encountered in polyimide insulators, which absorb water [15].

# **Experimental results**

In this section, experimental and simulated waveforms are compared in order to verify the validity of the previously described techniques. Guidelines are given for determining when skin effect and dielectric losses become important.

Measurements were made of signal propagation on a test structure with cross section corresponding to the transmission lines of type 2 in Table 2 above. The

calculated propagation delay  $\tau = \sqrt{LC}$  for these lines was 66 ps/cm. The high-speed test system shown schematically in Figure 5 [18] (using probes with 19-GHz bandwidth), with  $t_r = 33.4$  ps rise-time source and 10:1 coaxial probes (500- $\Omega$  input impedance), provided a quasi-open termination to the measured lines. They ranged in length from 0.8 to 20 cm and had impedance of 40 to 50  $\Omega$ . The results of measurements are shown in Figure 6. The input source signal (not shown), had an amplitude of 200 mV. All the output traces are shifted in time in order to emphasize the dispersion on long lines. As expected, quite large overshoots were encountered for short lines that were unclamped. It should be noted that these lines had a resistance one fiftieth of that of the onchip wiring.

607

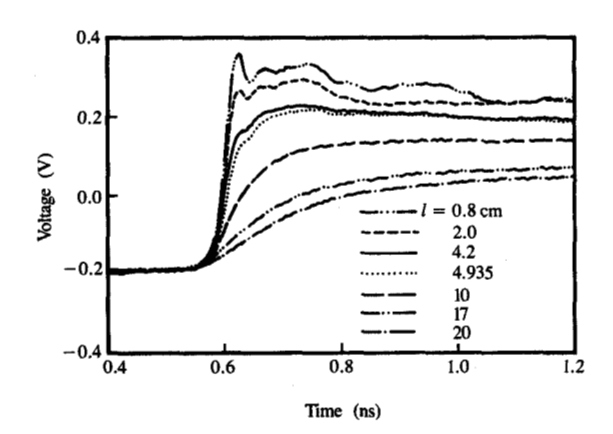
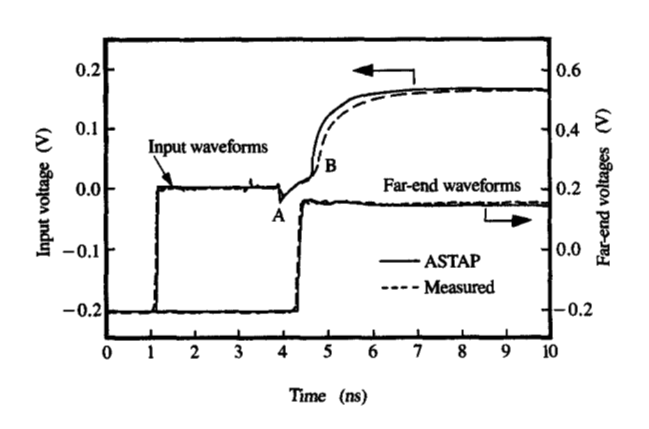


# Figure 6

Measured signals for lines with  $R_{\rm dc}=2.62~\Omega/{\rm cm}$ , lengths l=0.8 to 20 cm, and signal source (not shown) with  $t_{\rm r}=33.4~{\rm ps}$  and 200-mV swing. Measurements at far end of lines were made with 10:1 test probes.



Measured (dashed curves) and simulated (solid curves) waveforms for line with  $R_{\rm dc}=4~\Omega/{\rm cm}$  and length  $l=5.06~{\rm cm}$ , using 10:1 coaxial probes. Input monitored at sending oscilloscope channel; output measured at far end of line.

To aid in interpreting the time domain reflection (TDR) measurements, we can consider an approximation to the characteristic impedance of resistive lines. The characteristic impedance  $Z_0$ , given by (6), with series loss and G=0 can be expressed as follows:

$$Z_0 = \sqrt{\frac{L}{C} \left( 1 + \frac{R}{i\omega L} \right)}. \tag{19}$$

This expression can be approximated, for small losses, by

$$Z_{0} \cong \sqrt{\frac{L}{C}} \left( 1 - j \frac{R}{2\omega L} \right), \tag{20}$$

as shown in [3]. The impedance is then composed of a real part equal to the characteristic impedance without losses,  $\sqrt{L/C}$ , and a negative imaginary part corresponding to an equivalent capacitance given by

$$C_{\text{equiv}} = \frac{2L}{R} \sqrt{\frac{C}{L}}.$$
 (21)

Measured and simulated waveforms are shown in Figure 7 for a 5.06-cm-long transmission line with the triplate structure of type 3 shown in Table 2  $(R_{\rm dc} = 4 \ \Omega/{\rm cm})$ . The 500- $\Omega$  coaxial probes were used. The modeling used the equivalent circuit shown in Figure 5 and described in [18] for the test system. The agreement with test results is quite good. The coaxial probe tips, with  $L_p = 0.1625$  nH and  $C_p = 0.03$  pF, introduced a very small load on the test nodes. The input signal, sampled at the sending channel of a 20-GHz-bandwidth sampling oscilloscope, is almost doubled due to the quasi-open (500  $\Omega$ ) seen at the end of the line. The negative voltage step seen in reflection (TDR) on the input trace at point A in Figure 7 (after the delay through the connecting coaxial cables and probes) corresponds to the real part of the characteristic impedance  $Z_0$  seen at the beginning of the test line. The measured and simulated values for the real part of  $Z_0$  at point A were 45  $\Omega$  and 40  $\Omega$ , respectively. As the wave propagates farther down the line and its reflection returns to the input, the voltage rises to a value B (Figure 7), as would be expected due to the charging of the equivalent capacitance of Equation (21). The time span between points A and B represents the round-trip delay on the 5.06-cm line. The model calculations were based on the theoretical and numerical techniques described earlier and include frequency-dependent R and L due to skin effect and the calculated attenuation shown in Figure 4.

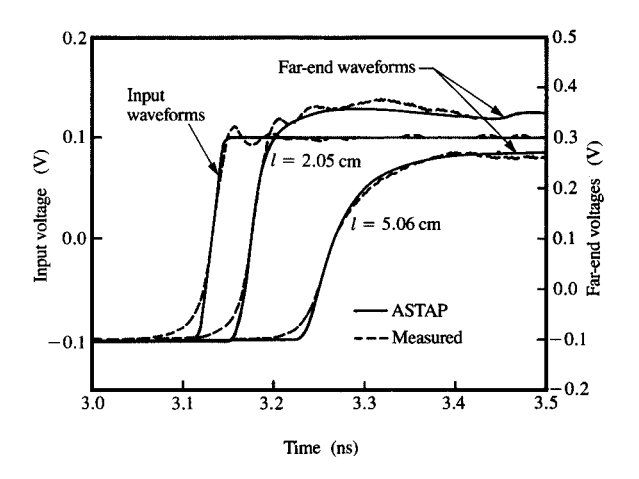
Figure 8 shows measured and simulated waveforms for pulse propagation on l=2.05-cm and 5.06-cm lines of type 3 shown in Table 2 with  $R_{\rm dc}=4~\Omega/{\rm cm}$ . The measured and simulated results for a 5.06-cm line are as follows: rise times  $t_{\rm r}=87~{\rm ps}$  and 90 ps, and propagation delays  $\tau=70~{\rm ps/cm}$  and 75 ps/cm, respectively. The input pulse with 33.4 ps rise time contains frequency components with significant energy around 10.5 GHz, which results in skin-effect-induced rise-time distortions. The excellent closeness of the experimental and simulated signal shapes confirms the validity of the analysis method. These measurements were performed with the step signal source provided by sampling oscilloscope systems. In actual chip-to-chip interconnections, both the rise time and the cycle time of

the transmitted signals are of interest. It is shown in [13] that in the case of narrow pulses (width less than twice the round-trip delay on the transmission line,  $W < 2\tau l$ ) propagating on long lossy lines, widening will occur due to the RC-like behavior predicted by (18). This distortion of narrow pulses can introduce additional delay, and skin effect must be included for accurate modeling of these effects, especially as computer cycle times become shorter.

To verify that dielectric loss is negligible, the modeling was repeated for the same 5.06-cm line with dielectric loss added. The modeled propagation delay obtained by using the attenuation values plotted as curve (d) in Figure 4 was 80 ps/cm, which was much higher than the measured delay of 70 ps/cm. The polyimide in our test structures clearly did not have a very high tan  $\delta_1$ . The calculation shows, however, that the 33.4 ps rise-time excitation can generate some dielectric-loss-induced dispersion. In the case of highly resistive interconnections, as discussed above, skin effect will dominate, and the dielectric loss can be ignored for most practical switching speeds encountered. In the case of wiring with small R, the dielectric loss should be included in the analysis. However, many packaging interconnection technologies use good dielectrics with very low tan  $\delta_1$ . For example, ceramic packages, as shown in Table 1, have resistance an order of magnitude lower than that of the lines measured in our study. It is shown in [19], however, that alumina can have tan  $\delta_1 = 0.0005$ , and mullite-type ceramics have tan  $\delta_1 = 0.0015$  to 0.0035, which are much lower than the losses encountered in organic dielectrics; therefore, dielectric dispersion can also be neglected for many ceramic packages.

#### • Skin-effect-induced dispersion

It is relevant to define the conditions for which skin effect becomes important for various technologies. It was shown earlier that in the case of on-chip wiring, the lines have very high resistive losses, but for the rise times of typical circuit technologies, the skin depth is much greater than the conductor cross sections, and current crowding, when  $\delta \ll t$ , comes into effect only at very high frequencies. In the case of chip-to-chip hybrid wiring such as thin-film conductors [16, 20-22], the resistive loss is smaller but still nonnegligible, especially since long interconnections are required. The conductors can have  $R_{dc}$  from 1 to 4  $\Omega$ /cm and thickness t of 5 to 8  $\mu$ m. The skin effect in these cases could become significant at frequencies greater than 0.9 to 3 GHz or rise times  $t_r$ , less than 116 to 398 ps (where  $\delta \leq t$ ). Practical switching speeds  $t_{\perp}$  of current circuits are in the range of 200 to 1000 ps; therefore, skin-effect-induced dispersion will degrade the signal rise times, but total circuit-to-circuit interconnection delays are not substantially increased.

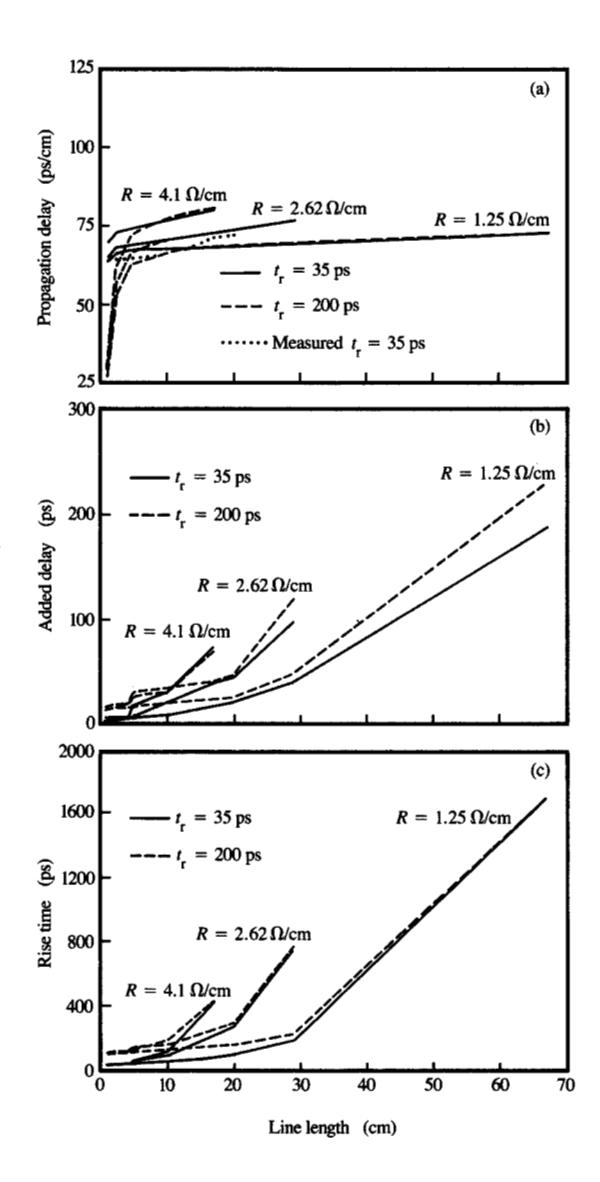


# Figure

Measured (dashed curves) and simulated (solid curves) waveforms for lines with  $R_{\rm dc}=4~\Omega/{\rm cm}$ , lengths  $l=2.05~{\rm cm}$  and 5.06 cm, and input source signal with 33.4-ps rise time. Signals at far end of lines tested with 10:1 probes.

In the case of printed circuit board interconnections, the cross sections are quite large, and the conductors have negligible resistance  $R_{\rm dc}$  of about 0.06  $\Omega/{\rm cm}$ , with t from 30 to 50  $\mu{\rm m}$ . The onset of skin effect can occur for rise times as slow as 7 ns; however, the attenuation at these speeds is only about 0.005 dB/cm, so dispersion is even less pronounced than for the type of interconnections discussed above. Modeling of signal propagation without frequency-dependent resistive losses will result in fairly accurate predictions for the typical lengths shown in Table 1.

Since skin effect influences primarily the highfrequency components, the upper portion of the pulse transitions is usually most rounded, as is illustrated in Figure 8. Delay is generally measured between the 50% levels of the driver circuit output and the receiver circuit input waveforms. The actual switching threshold of a receiver circuit, however, occurs in a band of about  $\pm 100$ mV around this level, which is a small fraction of the overall signal swing. This is generally caused by the device and package processing variations and power supply and temperature excursions. The signal rise time is defined between the 10% and 90% levels and is shown to be significantly affected by dispersion. The actual impact on digital circuit performance, however, is the additional delay as measured at the switching threshold band of the receiver circuit. If the slowdown of the upper portion of the signal transition begins to penetrate this band, considerable delay penalty is incurred.



#### Elallie C

(a) Modeling of propagation delays, (b) added path delays measured +100 mV above switching threshold, and (c) rise times as a function of line lengths for unterminated lines with  $R_{\rm dc}=1.25, 2.62$ , and  $4.1 \Omega/\text{cm}$  and for signal rise times  $t_{\rm r}$  of 35 ps and 200 ps. Dotted curve in part (a) shows measured delays for waveforms of Figure 6.

Modeling of signal propagation was done for the three types of transmission lines considered earlier in Figure 4 and Table 2, with  $R_{\rm dc} = 1.25$ , 2.6, and 4  $\Omega/{\rm cm}$ . The lines were driven by sources with rise times  $t_{\rm r}$  of 35 ps and 200 ps, and were terminated with Schottky barrier diode clamps (essentially in open-ended mode). Results are shown in **Figure 9**, as a function of line length.

Propagation delays were measured at the beginning and at the far end of the lines at the 50% signal levels. The rise times are shown for the signals at the end of the various lengths of transmission lines; the added delay penalty, as discussed above, was measured on the far-end signal between the 50% level and the +100-mV threshold point (positive-going transitions were used). In addition, in Figure 9(a), the dotted curve shows propagation delays (at 50% levels) measured on the test structures considered earlier in Figure 5 for the lines with  $R_{\rm dc} = 2.62~\Omega/{\rm cm}$  and using the high-input-impedance coaxial probes.

The lines with  $R_{\rm dc}=4~\Omega/{\rm cm}$  are analyzed for lengths up to 17 cm only, since the previous guideline suggests that  $l \leq 2Z_0/R=17.8~{\rm cm}$ . The added delay penalty would probably be significantly higher for the lines with  $R_{\rm dc}=4~\Omega/{\rm cm}$  than for the line with  $R_{\rm dc}=2.6~(l_{\rm max}=29~{\rm cm})$ , especially for  $t_{\rm r}=35~{\rm ps}$ , if these lines were used for  $l>l_{\rm max}$ . The guideline of  $l_{\rm max}=2Z_0/R$  ensures high-speed propagation on lossy lines. The rise-time degradation is the highest for  $t_{\rm r}=35~{\rm ps}$  and the highest  $R_{\rm dc}$ , but the added delay (231 ps), even for the longest lines ( $l=67~{\rm cm}$ ), is only 4.7% of the total circuit-to-circuit interconnection delay ( $\tau l=4.88~{\rm ns}$ ).

Typical rise times encountered in digital circuit interconnections will have frequency components that will be affected by skin effect ( $\delta \leq t$ , and increased high-frequency attenuation). In fact, thicker conductors will be affected at lower frequencies. If, however, the above restrictions on length are followed, the rise-time dispersion will minimally affect the parameter determining machine performance, which is the total path delay.

# Crosstalk on lossy transmission lines

A major concern in trying to increase interconnection density and switching speeds is the amount of crosstalk generated on quiet lines surrounded by active lines. The single-line analysis needs to be extended to coupled transmission lines. The differential equations (1) and (2) shown earlier for a uniform transmission line can be extended to (n + 1)-conductor parallel coupled lines, where V and I become *n*-dimensional vectors of the line voltages and currents [23, 24]. In this case, Z and Y are  $n \times n$  symmetric matrices, with frequency-dependent real and imaginary parts,  $Z = R + j\omega L$  and  $Y = G + j\omega C$ , where **R**, **L**, **G**, and **C** are also  $n \times n$  symmetric matrices. The solution to the differential equations has been presented in several publications, such as [23] and [24]. In order to use the same ASTAP program to perform transient analysis of the lossy coupled lines, we must specify the  $n \times n$  characteristic admittance matrix  $\mathbf{Y}_0 (\mathbf{Y}_0 = \mathbf{Z}^{-1} \mathbf{\Gamma})$ , the propagation matrix  $\mathbf{\Gamma}$ , and the eigenvectors **P** of  $\Gamma$  ( $\Gamma = \mathbf{P} \sqrt{\gamma} \mathbf{P}^{-1}$ , where  $\sqrt{\gamma}$  is the  $n \times n$  diagonal eigenvalue matrix of the product **ZY**).

The capacitance matrix C is calculated using the same program that was used for the single line [9]. The resistance and inductance matrices are obtained as functions of frequency using the numerical technique of [6] and Wheeler's rule in much the same way as was outlined earlier. In a typical interconnection application, X- and Y-directed lines are used. It is shown in [13, 14] that the presence of crossing orthogonal lines will slightly increase the self capacitance while significantly decreasing the mutual line capacitance. Then, three-dimensional capacitance and inductance modeling must be performed. The structures that we tested with X and Y wiring sandwiched between two reference planes were analyzed with the program described in [25], which is based on an electromagnetic solution using the method of moments with rooftop current approximations. Table 3 shows the measured and calculated change in self and mutual capacitances of X-layer conductors due to orthogonal Y-line loading. The 0%, 50%, and 100% loading conditions refer to absence of Y lines, Y lines at half the wiring density of the X lines, and Y lines at the same density as in the X-layer, respectively. The agreement between measurement and simulations is considered extremely good, given the uncertainty of the information available about the structure cross section and typical measurement accuracies.

In order to get the modeling results presented below, we used the same technique of modal decomposition built into the ASTAP program and described in [23] for n coupled lines. In order to give a better grasp of the physical phenomena involved in crosstalk, we focus on only two adjacent coupled lines and discuss the transfer of energy through capacitive and inductive coupling, which is a method that has been used extensively [26–28]. It is shown in these studies that the capacitive,  $K_C (-C_{12}/C_{11})$ , and inductive,  $K_L (L_{12}/L_{22})$ , couplings between adjacent lines add at the driving end and subtract at the far end of the line. The so-called near-end noise, NEN, can be approximated [26–28] by

$$NEN \cong K_{\rm B} 2\tau l V_{\rm in} / t_{\rm r}$$
 for  $l < t_{\rm r} / 2\tau$ . (22)

It saturates for  $l > t_r/2\tau$ , and becomes  $NEN \cong K_B V_{\rm in}$ .  $K_B$  is the backward-coupling coefficient  $[K_B = (K_C + K_L)/4]$ ,  $V_{\rm in}$  is the signal on the active line with rise time  $t_r$ ,  $\tau$  is propagation delay per unit length, and l is the length over which the two lines are adjacent, or the coupled length. It has been shown that NEN travels in the opposite direction from the active pulse and has a width equal to twice the line delay. In a homogenous medium, the farend noise (FEN) = 0. In most interconnection environments, inhomogeneities caused by vias, crossing lines, and dielectric interfaces give rise to far-end noise that travels in the direction of the active pulse, has a width equal to the rise time, and is always proportional

**Table 3** Change in self  $(C_{22})$  and mutual  $(C_{12})$  capacitance with orthogonal line loading.

Orthogonal loading (%)	Calculated (%)		Measured (%)	
	$\Delta C_{22}$	$\Delta C_{12}$	$\Delta C_{22}$	$\Delta C_{12}$
0	_		_	_
50	+7.9	-15.9	+7.2	-15.8
100	+15.8	-31.8	+15.3	-31.3

to the coupled length [24, 26-28]:

$$FEN \cong K_{\rm F} \tau l V_{\rm in} / t_{\rm r} \,, \tag{23}$$

where the forward-coupling coefficient,  $K_F$ , is  $(K_C - K_L)/4$ . The active signal has a finite rise time  $t_r$  in both (22) and (23). When open-ended transmission lines are used, the coupled noise doubles due to the positive reflection at the far end of the lines. Large overshoots, like the ones seen in Figure 6 on shorter lines, couple into quiet lines, creating greater crosstalk. On lossy coupled lines, however, crosstalk attenuates as well, and rise-time dispersion on the active lines results in less *NEN* and *FEN*, as can be seen from (22) and (23).

Measurements on coupled interconnections with lengths l from 0.8 to 20 cm were performed on pairs of lines with  $R_{dc} = 2.6 \Omega/\text{cm}$ , crossing orthogonal lines, and the triplate structure described earlier. The active line was open-ended and excited with a 35-ps rise-time signal. Testing was performed with the high-impedance probes described earlier, at the far end of the quiet line. That line was open at both ends, as shown schematically in Figure 5(b). Figure 10 shows three curves for two 17-cm coupled lines: (1) measured, (2) simulated, assuming constant resistive loss, and (3) simulated, assuming skin effect. The active line signal was monitored at the sending channel of the sampling oscilloscope, which was connected through coaxial cables and test probes to the input of the active line. The crosstalk waveform has the very fast negative-going far-end noise, FEN (input signal has rise time of 35 ps), followed by the wide near-end noise, which is reflecting back from the driving end after twice the line delay. Curves 1 and 3 agree fairly well, while curve 2 exhibits FEN that is 11 times larger than curve 3. It should be noted that even when the modeling is done with skin-effect losses (curve 3), there are some difficulties in calculating FEN accurately. This is due to the fact that  $K_F$  is proportional to the  $K_C - K_L$  difference, which requires calculation of very small differences between the eigenvalues of the propagation matrix  $\Gamma$ , as is explained in great detail in [24]. The capacitive coupling  $K_C$  was measured on the actual structure and agreed well with modeling, as can be seen in Table 3, while  $K_1$  was calculated based on the approximate

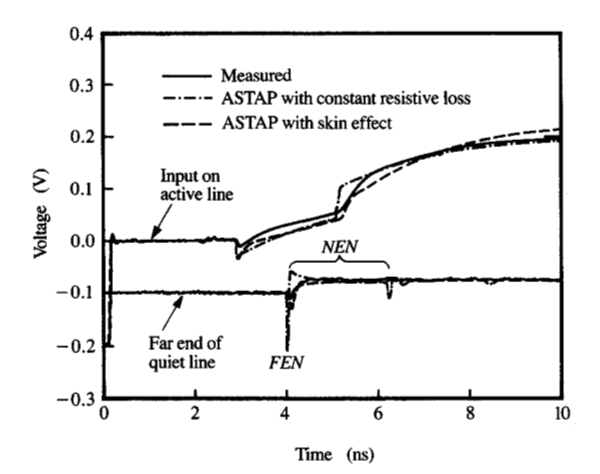


#### Figure 10

Input signals and noise on two 17-cm unterminated coupled lines with  $R_{\rm dc}=2.62\,\Omega/{\rm cm}$  and using the 10:1 probes with 35-ps rise-time source. Solid curves = measurements, dashed curves = simulations with skin effect, and dotted curves = simulations with constant resistive loss. Upper curves = input signals at near end of active line. Lower curves = far-end coupled noise (FEN) and reflected near-end noise (NEN) at far end of quiet line. Quiet line open-ended at both ends, as shown in Figure 5(b).

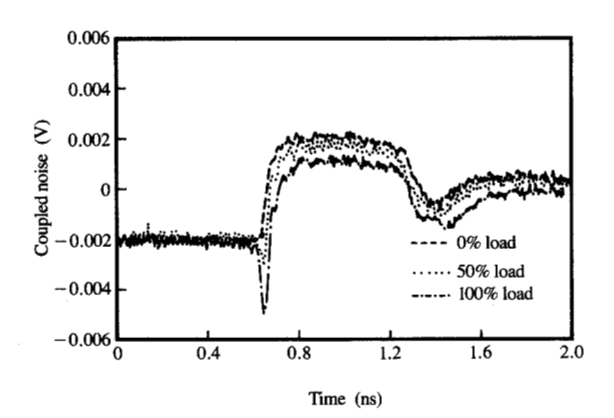


#### Figure 11

Expanded view of measured change in crosstalk as a function of orthogonal line loading for 4.935-cm lines with  $R_{\rm dc}=2.62~\Omega/{\rm cm}$ . Testing was done at far end of lines with 10:1 probes.

knowledge of the line cross sections. It was shown earlier in Figure 9 that skin-effect-induced dispersion did not substantially increase the chip-to-chip propagation delays, even for signals with 35-ps rise times. The measurements for Figure 10, on the other hand, show a significant decrease of the far-end coupled noise due to frequency-dependent losses. The narrow *FEN* pulse (35 ps wide) contains significant frequency components above 10 GHz, which are substantially attenuated.

The coupled noise is greatly affected by the capacitive loading of orthogonal lines in the adjacent layer. Using the results of Table 3, one finds that the capacitive coupling coefficient decreases from  $K_C = 0.1$  with no loading to  $K_C = 0.061$  with 100% loading. The near-end noise is expected to decrease, since it is proportional to  $K_C + K_L$ , while *FEN*, dependent on  $K_C - K_L$ , should increase. Figure 11 illustrates this effect for pairs of 4.935-cm-long coupled lines. Three traces show the measured coupled noise monitored at the far end of the quiet lines for crossing-line loading of 0%, 50%, and 100%. The test system is similar to the one described for the measurements of Figure 10. The quiet line is opencircuited at both ends, and the waveform monitored at the far end of the line shows both the narrow FEN and the wide NEN, due to the positive reflection from the end adjacent to the active line input.

To demonstrate the effect of signal rise times on coupled noise, an analysis was made using a source with 200-ps rise time (typical of a high-speed driver circuit) and 35-ps rise time. Modeling was done using ASTAP and the method described above for two coupled lossy transmission lines of type 2 in Table 2 ( $R_{dc} = 2.6 \Omega/\text{cm}$ ) with diode clamps at the end of the active line for a range of lengths l from 0.8 to 29 cm. Two types of circuit configurations were used to simulate typical conditions for worst-case near- and far-end crosstalk [14] encountered in high-performance digital computer circuits. Figure 12(a) simulates a quiet line with a receiver at the near end (high impedance) and an inactive, low-impedance driver at the far end, the condition for maximum NEN. Figure 12(b) has the reverse arrangement, for maximum FEN. Figure 13 plots the NEN and FEN results for the two excitation rise times. The crosstalk is expressed in percentage of the amplitude of the active line-driving signal.

Several conclusions can be drawn. In the case of lossy, unterminated, insufficiently clamped lines, overshoots on the active lines couple onto the adjacent, quiet lines, giving rise to large crosstalk for short lines, especially at fast rise times. For signal rise times that are slower than 200 ps, the NEN and FEN are similar in magnitude, and it was found that for this case, the constant-resistance model produced results almost identical to those of the frequency-dependent skin-effect analysis. As the rise times become faster ( $t_r < 200$  ps), FEN will dominate, and it is extremely important to take skin effect into account. The far-end noise, having a width equal to the signal rise time, as shown earlier, will contain high-

frequency components, which will be strongly attenuated. This explains why the far-end noise increases in length up to a point and then starts decreasing for very long lines.

#### **Discussion and conclusions**

Here we review the significance of the different loss mechanisms that have been analyzed. In the case where  $R \times l_{\text{max}} \ll Z_0 \ (R \times l_{\text{max}} \le 0.1 \ Z_0)$ , interconnection transmission lines may be considered lossless and will transmit signals with negligible distortion. Such is the case with wide (60–100  $\mu$ m) and thick (30–50  $\mu$ m) printed-circuit-board wirings. These lines are generally terminated to avoid reflections, and the amplitude is only reduced by the dc drop. Skin effect will be present for rise times less than 7 ns; however, due to the very low  $R_{dc}$ shown in Table 1, it will create insignificant dispersion. Dielectric loss will dominate in this environment if very fast rise-time signals are sent on these lines. The discontinuities due to capacitive loadings of crossing lines and very long and coarse vias generally tend to distort and slow down the signals well before any frequencydependent losses come into play.

Thick-film ceramic carriers have finite series loss, since  $R \times l_{\text{max}} \leq 0.2Z_0$ , and some rise-time distortion will be encountered. This type of wiring uses fairly thick lines (16–25  $\mu$ m), and skin-effect onset will occur with signals of around 1 ns rise time. However, distortion will be minimal because of the low  $R_{\text{dc}}$ . Dielectric loss could play a strong role, though most ceramics have been shown to have very low tan  $\delta_1$ . The line and via loadings, in this case as well, will introduce most of the rise-time distortion.

Thin-film carriers have substantial series loss, since  $R \times l_{\text{max}}$  can be in the range  $0.5Z_0$  to  $2Z_0$ . In order to use such wiring to propagate fast rise-time signals, the transmission lines are unterminated, and a controlled amount of attenuation can be tolerated because of the voltage doubling at the open end. Rise-time dispersion will occur, even for frequency-independent resistive loss. The conductors generally used are fairly thin  $(5-8 \mu m)$ , so that skin-effect onset occurs only for faster rise times of  $t_r < 100$  ps. Due to the high  $R_{de}$ , skin effect will dominate and dielectric loss can generally be ignored. Since such interconnections can propagate fast signals, the switching speeds will be limited by the noise margin of digital receiver circuits. For typical systems, crosstalk and power-supply noise generated by the simultaneous switching of many drivers will limit the transitions to not less than 200 ps. Finally, on-chip wires are very resistive but use very thin conductors  $(1-1.4 \mu m)$ , so that skineffect onset occurs at extremely fast rise times, approaching 10 ps. The high series resistance, capacitive loadings of orthogonal lines, and increase in inductance due to power bus layouts can significantly slow down the

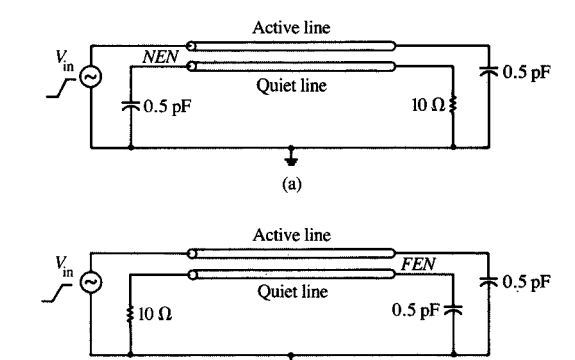


# Figure 12

Circuit configurations for analyzing worst-case crosstalk in computer applications. (a) Near-end coupled noise, NEN; (b) far-end coupled noise, FEN. Uses high impedance at receiver input (C=0.5 pF) and low-impedance, quiet driver ( $10~\Omega$ ).

(b)

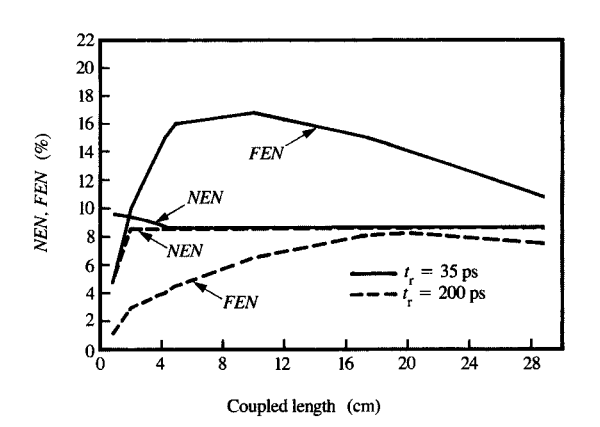


#### Figure 13

Simulated *NEN* and *FEN* crosstalk for signal rise times  $t_{\rm r}$  of 35 ps (solid curves) and 200 ps (dashed curves), and for lines with  $R_{\rm dc}=2.62~\Omega/{\rm cm}$  clamped with Schottky barrier diodes. Crosstalk is expressed in percentage of active line-driving signal amplitude.

on-chip communications, especially as chip sizes increase. On-chip wiring will use planar topographies and transmission line structures in the future to avoid these problems.

In conclusion, we state that a detailed modeling method was given for including frequency-dependent

losses, such as skin effect and dielectric dispersion, in high-speed transient analyses. The available tools and their relevance to this type of study were explained. Accurate predictions require including all the loss mechanisms. It is believed, however, that it is sufficient to use frequency-independent series loss in modeling risetime dispersion and coupled noise for a large group of interconnection types. This simplification will probably remain valid for many years to come, since practical limitations restrict possible switching speeds. Guidelines were given concerning the range of frequencies (switching speeds), densities (cross-sectional dimensions), and wiring lengths where severe dispersion can affect the circuit path delays in high-performance computers, for thin- and thick-film interconnection technologies that are in use or in development. Waveforms measured on experimental transmission line structures demonstrated the reflections, crosstalk, and rise-time slowdown encountered on lossy lines, and they showed very good agreement with simulations. We conclude that lossy, unterminated transmission lines can be used successfully to propagate high-speed signals when the amount of allowed loss is less than given design guidelines.

#### References

- J. K. Hagge, "Ultra-Reliable Packaging for Silicon-on-Silicon WSI," Proceedings of the 38th Electronic Components Conference, ECC'88, 1988, pp. 282–292.
- R. R. Tummala and E. J. Rjmaszewski, Microelectronics Packaging Handbook, Van Nostrand Reinhold, New York, 1989
- R. E. Matick, Transmission Lines for Digital and Communication Networks, McGraw-Hill Book Co., New York, 1969
- 4. R. E. Collin, *Field Theory of Guided Waves*, McGraw-Hill Book Co., New York, 1960, pp. 124–125.
- 5. H. A. Wheeler, "Formulas for the Skin Effect," *Proc. IRE*, pp. 412–424 (1942).
- W. T. Weeks, L. L. Wu, M. F. McAllister, and A. Singh, "Resistive and Inductive Skin Effect in Rectangular Conductors," *IBM J. Res. Develop.* 23, 652–660 (1979).
- M. V. K. Chari and P. O. Silveter, Finite Elements and Magnetic Field Problems, John Wiley & Sons, Inc., New York, 1979.
- O.-K. Kwon, R. Fabian, and R. F. W. Pease, "Closely Packed Microstrip Lines as Very High-Speed Chip-to-Chip Interconnects," *IEEE Trans. Components, Hybrids, Manuf. Technol.* CHMT-10, 314–320 (1987).
- W. T. Weeks, "Calculation of Coefficients of Capacitance of Multiconductor Transmission Lines in the Presence of a Dielectric Interface," *IEEE Trans. Microwave Theory Tech.* MTT-18, 35-43 (1970).
- C. S. Chang, "Electrical Design of Signal Lines for Multilayer Printed Circuit Boards," *IBM J. Res. Develop.* 32, 647–657 (1988).
- E. Weber, Linear Transient Analysis, Vol. II, John Wiley & Sons, Inc., New York, 1956, pp. 381–384.
- C. W. Ho, D. A. Chance, C. H. Bajorek, and R. E. Acosta, "The Thin Film Module as a High-Performance Semiconductor Package," *IBM J. Res. Develop.* 26, 286–296 (1982).
- A. Deutsch and C. W. Ho, "Triplate Structure Design for Thin Film Lossy, Unterminated Lines," *Proceedings of the 1981 IEEE International Symposium on Circuits and Systems*, 1981, pp. 1-5.

- A. Deutsch and C. W. Ho, "Thin Film Interconnection Lines for VLSI Packaging," Proceedings of the IEEE International Conference on Computer Design, ICCD'83, 1983, pp. 222–226.
- Advanced Statistical Analysis Program (ASTAP), Program Reference Manual, Order No. SH20-1118-0; available through IBM branch offices. W. T. Weeks, A. J. Jimenez, G. W. Mahoney, D. Metha, H. Qassemzadeh, and T. R. Scott, "Algorithms for ASTAP—A Network Analysis Program," IEEE Trans. Circuit Theory CT-20, 628-634 (1973).
- T. Watari and H. Murano, "Packaging Technology for the NEC SX Supercomputer," *IEEE Trans. Components, Hybrids,* Manuf. Technol. CHMT-8, 462-467 (1985).
- 17. L. B. Rothman, "Properties of Thin Polyimide Films," J. Electrochem. Soc. 127, 2216-2220 (1980).
- V. A. Ranieri, A. Deutsch, G. Arjavalingam, and G. V. Kopcsay, "A Novel 24 GHz Bandwidth Coaxial Probe," *IEEE Trans. Instr. Meas.* 39, 504–507 (1990); V. A. Ranieri, A. Deutsch, G. Arjavalingam, and G. V. Kopcsay, "Versatile High Speed Coaxial Probes for Package and Device Testing," *IBM Tech. Disclosure Bull.* 32, 133–135 (1980).
- M. Horiuchi, K. Mizushima, Y. Takeuchi, and S.-I. Wakabayashi, "New Mullite Ceramic Packages and Substrates," *IEEE Trans. Components, Hybrids, Manuf. Technol.* 11, 439–446 (1988).
- T. A. Lane, F. J. Belcourt, and R. J. Jensen, "Electrical Characteristics of Copper/Polyimide Thin Film Multilayer Interconnects," *Proceedings of the 37th Electronic Components Conference, ECC'87*, 1987, pp. 614–621.
- C. C. Chao, K. D. Scholz, J. Leibovitz, M. L. Cobarruviaz, and C. C. Chang, "Multilayer Thin-Film Substrate for Multichip Packaging," *Proceedings of the 38th Electronic Components Conference*, ECC'88, 1988, pp. 276–281.
- S. Sasaki, T. Kon, and T. Ohsaki, "A New Multi-Chip Module Using a Copper Polyimide Multi-Layer Substrate," *Proceedings* of the 39th Electronic Components Conference, ECC'89, 1989, pp. 629-635.
- 23. A. J. Gruodis and C. S. Chang, "Coupled Lossy Transmission Line Characterization and Simulation," *IBM J. Res. Develop.* 25, 25–41 (1981).
- C. S. Chang, "Transmission Lines," Advances in CAD for VLSI, 3, Part II, Circuit Analysis, Simulation and Design, A. E. Ruehli, Ed., North-Holland Publishing Co., Amsterdam, 1987, pp. 292-332.
- B. J. Rubin, "Modeling of Arbitrarily Shaped Signal Lines and Discontinuities," *IEEE Trans. Microwave Theory Tech.* 37, 1057–1060 (1989).
- A. Feller, H. R. Kaupp, and J. J. Digiacomo, "Crosstalk and Reflections in High Speed Digital Systems," *Proceedings of the Fall Joint Computer Conference*, December 1965, pp. 511–525.
- N. C. Arvanitakis, J. T. Kolias, and W. Radzelovage, "Coupled Noise Prediction in Printed Circuit Boards for a High-Speed Computer System," Proceedings of the 7th International Electronic Circuit Packaging Symposium, August 1966, pp. 1-11.
- C. S. Chang, G. Crowder, and M. F. McAllister, "Crosstalk in Multilayer Ceramic Packaging," *Proceedings of the 1981 IEEE International Symposium on Circuits and Systems*, 1981, pp. 6-11.

Received July 5, 1989; accepted for publication January 26, 1990

Alina Deutsch 1BM Thomas J. Watson Research Center, P.O. Box 218, Yorktown Heights, New York 10598. Mrs. Deutsch received the B.S. and M.S. degrees in electrical engineering from Columbia University and from Syracuse University, respectively. She joined IBM in 1971 and has since worked in several areas, including testing of semiconductor and magnetic bubble memory devices. She is an advisory engineer currently working on the design, analysis, and testing of packaging structures for future high-end machine applications. Mrs. Deutsch has written many technical papers and holds several patents. She is a member of the Institute of Electrical and Electronics Engineers, Tau Beta Pi, and Eta Kappa Nu.

Gerard V. Kopcsay IBM Thomas J. Watson Research Center, P.O. Box 218, Yorktown Heights, New York 10598. Mr. Kopcsay is a Research Staff Member in the Packaging Technology Department at the IBM Thomas J. Watson Research Center. Since joining IBM Research in 1978, he has been working on the analysis and design of high-performance computer packaging. From 1969 to 1978 he worked on research and development of low-noise microwave receivers at the AIL Division of Eaton Corp. Mr. Kopcsay holds the B.E. and M.S. degrees in electrical engineering; he is a member of the Institute of Electrical and Electronics Engineers and the American Physical Society.

Vincent A. Ranieri formerly of IBM Thomas J. Watson Research Center, P.O. Box 218, Yorktown Heights, New York 10598; now retired. Mr. Ranieri joined IBM in 1955 at Poughkeepsie, New York, and was with the Research Division from 1961 until his retirement in 1990. He worked in several areas, including the testing and fabrication of magnetic memories and electromigration life testing and analysis of many alloys. Mr. Ranieri co-authored several papers and patent disclosures.

- J. K. Cataldo IBM Thomas J. Watson Research Center, P.O. Box 218, Yorktown Heights, New York 10598.
- **E. A. Galligan** *IBM Thomas J. Watson Research Center, P.O. Box 218, Yorktown Heights, New York 10598.*
- W. S. Graham 1BM Thomas J. Watson Research Center, P.O. Box 218, Yorktown Heights, New York 10598.
- R. P. McGouey IBM Thomas J. Watson Research Center, P.O. Box 218, Yorktown Heights, New York 10598.

Sharon L. Nunes IBM Thomas J. Watson Research Center, P.O. Box 218, Yorktown Heights, New York 10598. Dr. Nunes received her Ph.D. in polymer science from the University of Connecticut in 1983. She is currently manager of the Thin Film Structures group at the IBM Thomas J. Watson Research Center. She has worked in the area of thin films materials and processing for the past four years. Prior to her assignment in research, she was responsible for materials selection and characterization in the Electronics Packaging Lab in Rochester, Minnesota. Dr. Nunes is a member of the Society of Plastics Engineers and is on the Board of Directors of the Plastics Analysis Division of SPE.

Jurij R. Paraszczak IBM Thomas J. Watson Research Center, P.O. Box 218, Yorktown Heights, New York 10598. Dr. Paraszczak received his B.S. and Ph.D. in chemistry from Sheffield University in 1973 and 1976, respectively. He is currently manager of the thin films application area at the IBM Thomas J. Watson Research Center. He has worked in the field of lithography and plasma

processing since joining IBM in 1979. His previous work has included electron-beam lithography, semiconductor etching, and the design and use of microwave plasmas in semiconductor processing, with particular application to multilayer resist systems. Dr. Paraszczak is a member of the Institute of Electrical and Electronics Engineers and Sigma Xi.

- J. J. Ritsko IBM Thomas J. Watson Research Center, P.O. Box 218, Yorktown Heights, New York 10598.
- R. J. Serino IBM Thomas J. Watson Research Center, P.O. Box 218, Yorktown Heights, New York 10598.
- **D. Y. Shih** 1BM Thomas J. Watson Research Center, P.O. Box 218, Yorktown Heights, New York 10598.
- J. S. Wilczynski IBM Thomas J. Watson Research Center, P.O. Box 218, Yorktown Heights, New York 10598.